iScience

Article

HucMSCs can alleviate abnormal vasculogenesis induced by high glucose through the MAPK signaling pathway

Graphical abstract

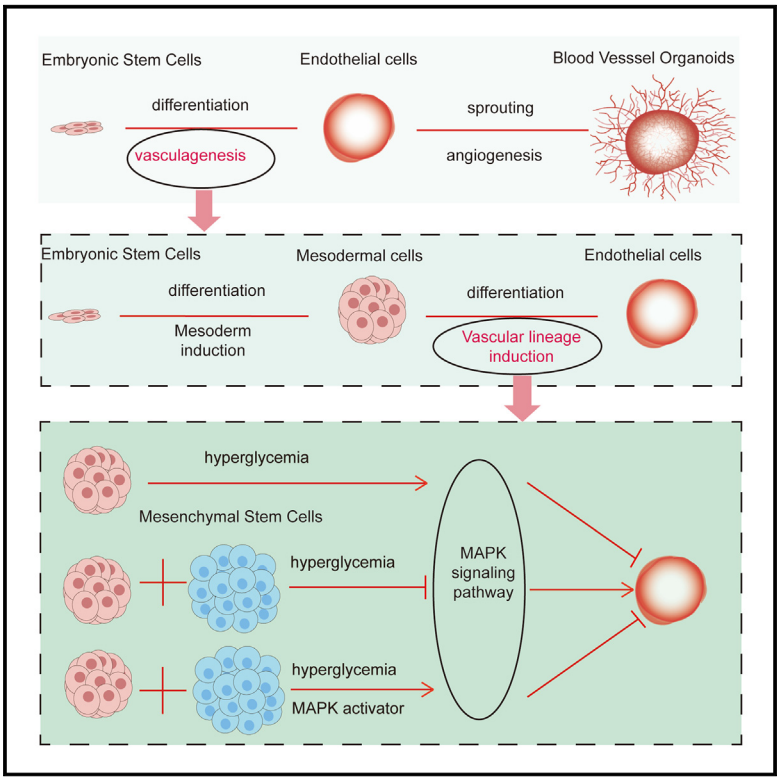

Highlights

- The induction process of BVOs can be divided into vasculogenesis and angiogenesis
- The formation of VI-BVOs is more vulnerable to damage from high glucose than MI-BVOs
- HucMSCs can improve vasculogenesis through the MAPK signaling pathway

Authors

Yang Yao, Tiantian Shan, Xiaoying Li

Correspondence

yingbaby1010@163.com

In brief

Pathophysiology; Stem cells research; Vascular remodeling

Yao et al., 2024, iScience 27, 111354
December 20, 2024
https://doi.org/10.1016/j.isci.2024.111354

CellPress

iScience

CellPress
OPEN ACCESS

Article

HucMSCs can alleviate abnormal vasculogenesis induced by high glucose through the MAPK signaling pathway

Yang Yao,[1,2] Tiantian Shan,[2,3] and Xiaoying Li[2,4,5,6,*]

[1]Department of Anesthesiology, Qingdao Municipal Hospital, School of Medicine, Qingdao University, Qingdao 266011, China
[2]Research Center of Translational Medicine, Central Hospital Affiliated Shandong First Medical University, Jinan 250013, China
[3]Department of Cardiology, The Affiliated Hospital of Qingdao University, Qingdao 266000, China
[4]Department of Emergency, Jinan Central Hospital, Jinan 250013, China
[5]Department of Emergency, Central Hospital Affiliated Shandong First Medical University, Jinan 250013, China
[6]Lead contact
*Correspondence: yingbaby1010@163.com
https://doi.org/10.1016/j.isci.2024.111354

SUMMARY

Vascular complications caused by diabetes mellitus contribute a major threat to increased disability and mortality of diabetic patients, which are characterized by damaged endothelial cells and angiogenesis. Human umbilical cord-derived mesenchymal stem cells (hucMSCs) have been demonstrated to alleviate endothelial cell damage and improve angiogenesis. However, these investigations overlooked the pivotal role of vasculogenesis. In this study, we utilized blood vessel organoids (BVOs) to investigate the impact of high glucose on vasculogenesis and subsequent angiogenesis. We found that BVOs in the vascular lineage induction stage were more sensitive to high glucose and more susceptible to affect endothelial cell differentiation and function. Moreover, hucMSCs can alleviate the high glucose-induced inhibition of endothelial cell differentiation and dysfunction through MAPK signaling pathway downregulation, with the MAPK activator dimethyl fumarate further illustrating the results. Thereby, we demonstrated that high glucose can lead to abnormal vasculogenesis and impact subsequent angiogenesis, and hucMSCs can alleviate this effect.

INTRODUCTION

Diabetes mellitus is a globally prevalent chronic disease characterized by hyperglycemia with an increasing incidence in the general population. Currently, 537 million people worldwide are living with diabetes mellitus, and this number may reach 700 million by 2045.[1] Various vascular complications caused by long-term hyperglycemia, such as cardiovascular disease (CVD), diabetic kidney disease (DKD), diabetic retinopathy (DR), and neuropathy, are major contributors to the increased morbidity and mortality and reduced quality of life of patients with diabetes mellitus.[2]

Many studies have demonstrated that endothelial dysfunction causes vascular complications.[3] Endothelial cells (ECs) line the inner surface of blood vessels and form a selective biological barrier that works to maintain vascular homeostasis by regulating blood transport, fibrinolysis, macromolecule metastasis, and immune responses and is involved in inflammatory responses.[4] Long-term exposure to high-glucose conditions can decrease endothelial cell viability, increase vascular permeability, and accelerate endothelial cell apoptosis and aging, resulting in abnormal angiogenesis and poor damage repair.[5,6] To date, conventional research and therapeutic approaches have focused mainly on maintaining a normal blood glucose level and regulating the proliferation and migration of endothelial cells to improve angiogenesis and the repair of the vasculature,[7] however, the related studies overlooked the pivotal role of vasculogenesis.

In fact, the establishment of the vascular system is divided into two stages: vasculogenesis and angiogenesis.[8] Vasculogenesis refers to the formation of the initial vascular network *in situ* through the differentiation, expansion, and merging of mesodermal precursor-derived endothelial precursors (EPCs) during embryonic development.[9] Angiogenesis further occurs in the initial vascular network via sprouting or splitting.[10] Therefore, abnormal vasculogenesis inevitably leads to abnormal angiogenesis and vascularization. *In vitro* whole-embryo culture models allow the study of this critical developmental period, and research indicates that short-term high blood glucose is teratogenic, leading to dose-dependent growth retardation, neural tube damage, and yolk sac failure.[11] Research also indicates that vasculogenesis is related to many proteins, such as hypoxia-inducible factor 1 (HIF-1) and vascular endothelial growth factor (VEGF), which are active during normal vasculogenesis and are downregulated in hyperglycemia.[12] In addition, apoptosis signal regulating kinase 1 (ASK1) is upregulated by high glucose conditions, and vascular damage can be abolished when the related downstream events are inhibited.[13] Thioredoxin-1, an

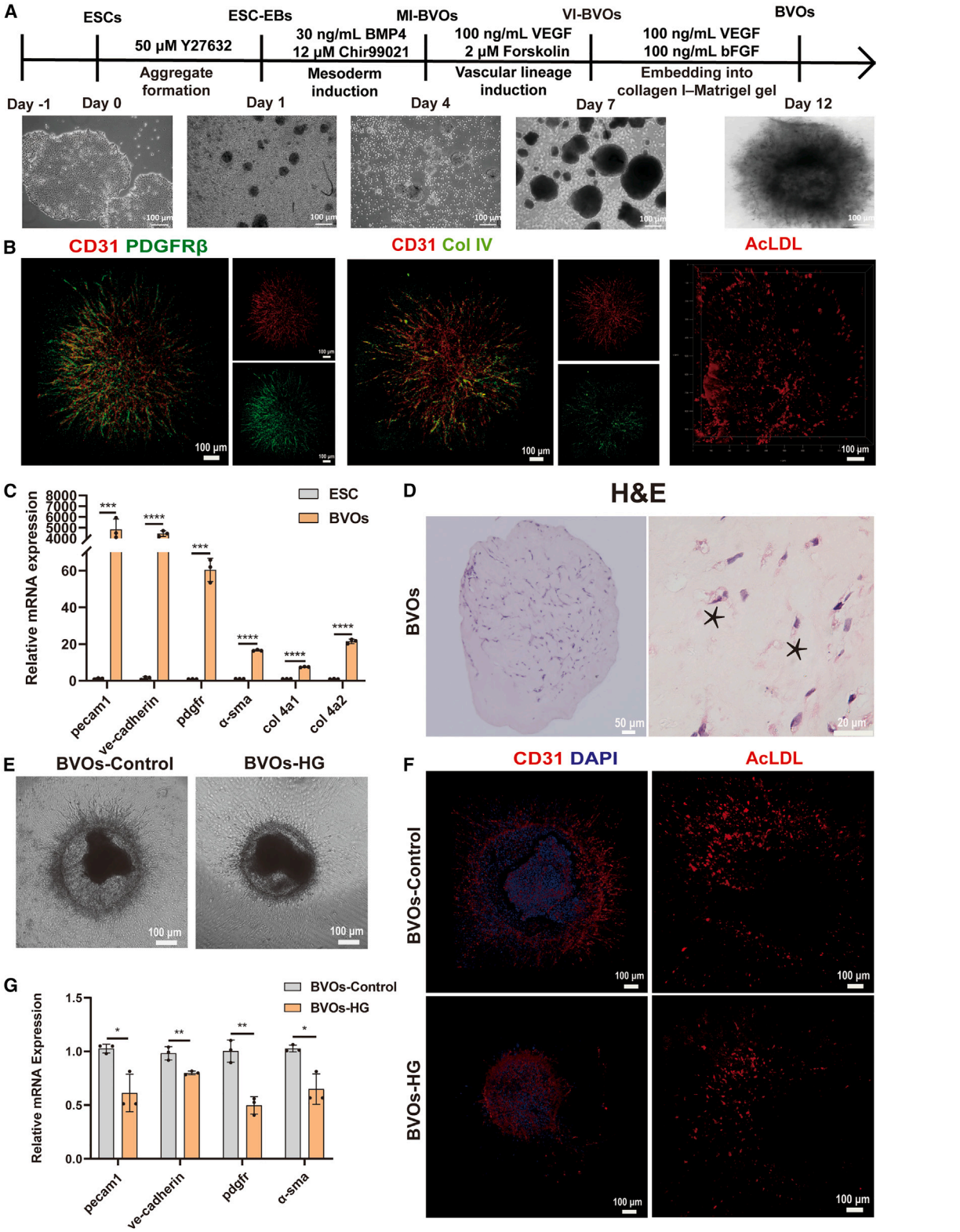

(legend on next page)

inhibitor of ASK1, and nitric oxide can modulate murine yolk sac vasculogenesis and reverse glucose-induced vasculopathy.[12,14] In addition, in adult tissues, vasculogenesis occurs can repair vascular damage through the differentiation of EPCs into endothelial cells. EPCs can also serve as biomarkers of cardiovascular risk.[15]

Despite the knowledge gained from studies in mouse embryos that has provided a preliminary theoretical basis for the abnormal vasculogenesis caused by high glucose conditions, the regulatory molecules and signaling events underlying vessel development and patterning remain largely unknown. Considering the complexity of embryonic tissue and species differences in animal models and humans, it is difficult to directly translate the results of animal experiments to humans. Thus, models of organoids derived from stem cells can be important complementary tools for understanding this crucial period of human development.

Blood vessel organoids (BVOs) are generated from embryonic stem cells (ESCs) or pluripotent stem cells (PSCs). After mesoderm induction and vascular lineage induction stages, BVOs with vascular network-like structures ultimately form in the collagen-Matrigel hydrogel.[16,17] BVOs exhibit a stable vascular structure, a dense vascular network, and intricate cellular interplay; thus, as vascular models, they are superior to other types of models for *in vitro* studies. As our understanding of BVOs has continued to evolve, we have found that the induction stage of BVOs has characteristics similar to those of vasculogenesis and angiogenesis in the native vasculature *in vivo*. Therefore, BVOs are highly important for elucidating the mechanism by which high glucose induces vascular abnormalities and for developing treatments.

Recently, stem cell therapy has provided a new therapeutic strategy for diabetes, and various types of stem cells, most commonly human umbilical cord-derived mesenchymal stem cells (hucMSCs), have been widely used in the clinical treatment of diabetes.[18,19] Animal experiments and clinical practice have shown that hucMSCs can decrease blood glucose and HbA1c levels by releasing extracellular vesicles, exosomes, growth factors, chemokines, and cytokines to modulate immune responses and repair injured tissues.[20] However, the effect of hucMSCs on abnormal vasculogenesis is unclear.

In this study, we tested and characterized BVOs at different induction stages. The induction stage is divided into two phases: vasculogenesis and angiogenesis. By high-glucose exposure of BVOs at different induction stages, we identified that vascular lineage induction stage was the most sensitive to high-glucose conditions. To explore the effect of hucMSCs on vasculogenesis in a high-glucose environment, we cocultured hucMSCs with BVOs in the vascular lineage induction stage in high-glucose medium. Subsequently, we investigated the mechanisms by which high glucose and hucMSCs affect vasculogenesis. Our findings provide a theoretical basis for the mechanism underlying diabetic vasculogenesis and for drug and other therapeutic approaches to address the related abnormalities. Moreover, we provide an idea for the study of not only BVOs but also other organoids of the corresponding organs.

RESULTS

Generation of BVOs and exploration of the effects of high-glucose conditions on angiogenesis in BVOs

BVOs were generated from the hESC line H9 according to the protocol described by Wimmer et al.[17] Following mesoderm and vascular linage induction, VI-BVOs were embedded in collagen I-Matrigel (3:1) hydrogels. After embedding, robust endothelial networks sprouted from the VI-BVOs; the resulting structures were called BVOs (Figure 1A). To determine the cellular composition of the BVOs, we conducted whole-mount staining for vascular markers associated with endothelial cells (ECs), pericytes (PCs), smooth muscle cells (SMCs) and the basement membrane (BM). $CD31^+$ ECs and $PDGFR\beta^+$ PCs were in intimate contact with each other and were typically encapsulated within the Col IV^+ BM (Figure 1B). Moreover, the BVOs could internalize DiI-labeled Ac-LDL (DiI-Ac-LDL), a characteristic function of endothelial cells (Figure 1B). Notably, the upregulated gene expression of EC, PC and BM markers corroborated the successful differentiation within the BVOs (Figure 1C). Ultrastructural analysis via HE staining revealed the formation of lumens within the BVOs (Figure 1D). Our results validated the effective generation of BVOs, which exhibited structural and functional features reminiscent of those of the native vasculature. Moreover, to test whether BVOs can simulate abnormal angiogenesis in high-glucose environments, after VI-BVOs were embedded in the hydrogel on the first day we treated them with control medium (BVOs-Control) or high-glucose medium (BVOs-HG), as described in the literature.[16] By inverted phase contrast microscopy, we found that on the third day of embedding, high-glucose medium significantly inhibited the

Figure 1. Generation of BVOs and exploration of the effects of high-glucose conditions on angiogenesis in BVOs

(A) Schematic representation of the process for generating BVOs derived from human ESCs.

(B) BVOs displayed CD31 staining as a marker of endothelial cells, PDGFR-β staining as a marker of pericytes, and Col IV staining as a marker of the basement membrane. Moreover, BVOs were able to take up DiI-Ac-LDL.

(C) The gene expression levels of *Pecam1, VE-Cadherin, Pdgfr, α-Sma, Col 4a1* and *Col 4a2* in BVOs were higher than those in ESCs.

(D) HE staining visualized the lumen (*) of BVOs.

(E) Inverted phase contrast images of VI-BVOs on day 3 after embedding in the hydrogel: control medium group (BVOs-Control) and high-glucose medium group (BVOs-HG).

(F) Compared to those in the BVOs-Control group, the CD 31 expression levels and acLDL uptake function of endothelial cells in the BVOs-HG group were significantly decreased.

(G) Compared to those in the BVOs-Control group, the expression of the endothelial cell marker genes Pecam1/VE-cadherin and the pericyte marker genes Pdgfr/α-sma in the BVOs-HG group was significantly downregulated in the BVOs-HG group. For (C) and (G), data are represented as mean ± SD. ($n = 3$ replicates per condition from 3 independent experiments, $^*p < 0.05$, $^{**}p < 0.01$, $^{***}p < 0.001$, $^{****}p < 0.0001$ from two-tailed Student's *t* test)(Scale bar: A, B, E, F = 100 μm, D (left) = 50 μm, D (right) = 20 μm).

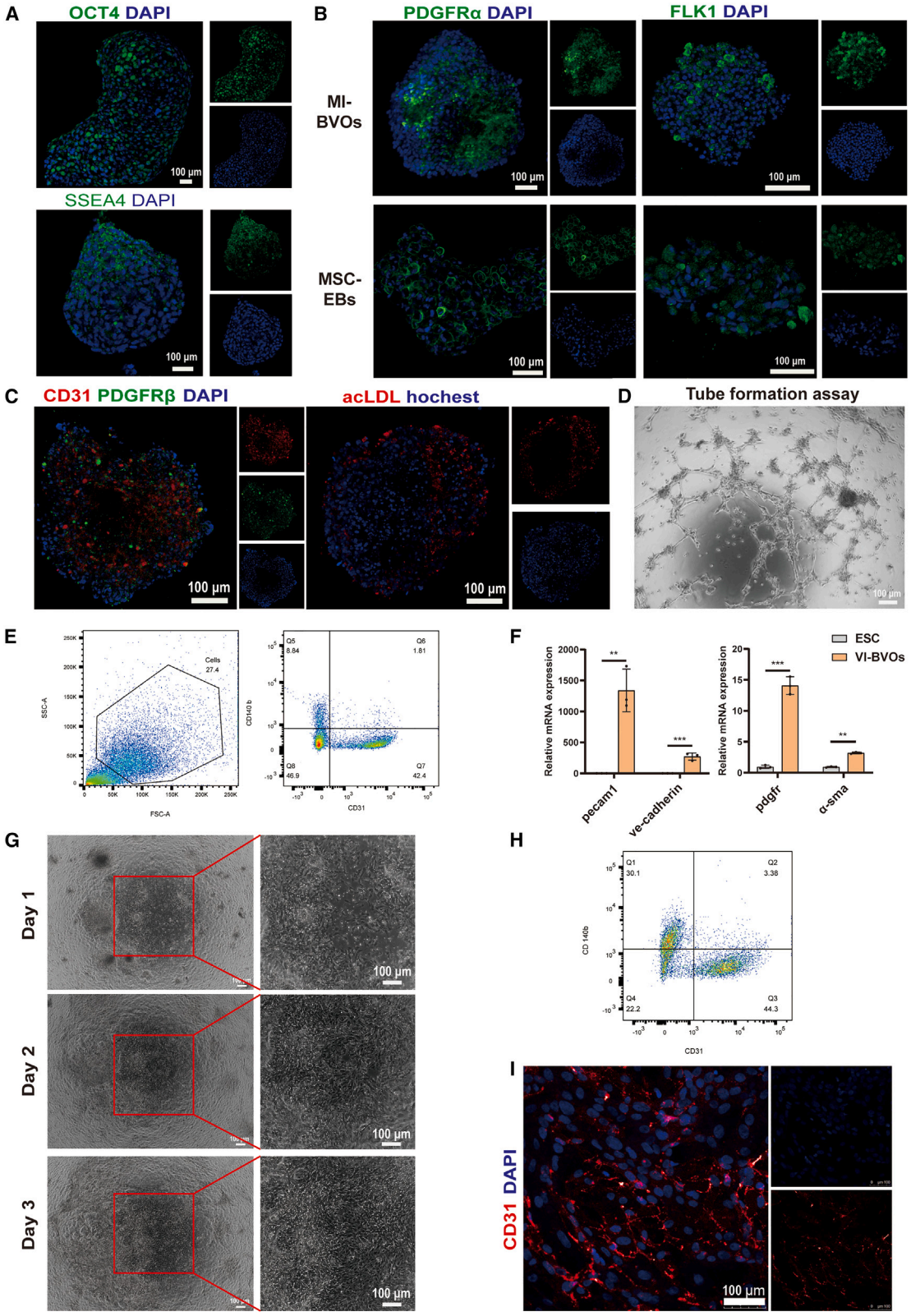

(legend on next page)

sprouting of BVOs (Figure 1E). Moreover, the immunofluorescence staining results demonstrated that the differentiation levels of CD31$^+$ endothelial cells was downregulated and ac-LDL uptake was inhibited (Figures 1F and S1)). The downregulated gene expression of vascular markers was consistent with the immunofluorescence staining results (Figure 1G), both of which indicated that high-glucose conditions can impair angiogenesis in BVOs. The above results demonstrated that we successfully constructed BVOs and that our model can simulate the process of angiogenic impairment caused by high glucose. In the following studies, we explored whether BVOs can simulate vasculogenesis and the effect of high glucose on vasculogenesis.

BVOs induction can be divided into two phases: Vasculogenesis and angiogenesis

During embryonic development, the formation of the vascular system occurs in two phases: vasculogenesis and angiogenesis. According to the induction protocol and characterization of BVOs, we hypothesized that the process of BVOs induction could also be divided into phases of vasculogenesis and angiogenesis. To investigate whether BVOs can simulate vasculogenesis, we detected and analyzed characteristic markers of the mesoderm and vascular lineage corresponding to different induction stages in BVOs at the transcriptional and translational levels. We first evaluated the expression of stemness markers in ESC-EBs, and the immunofluorescence staining results showed that ESC-EBs were composed of many OCT4+ and SSEA4+ ESCs, which provide a solid foundation for the successful generation of BVOs (Figure 2A). After three days of treatment with BMP4 and CHIR99021, MI-BVOs had characteristics of mesoderm cells, relative to hucMSC-EBs, both contained PDGFRα+ and FLK1+ mesodermal cells (Figure 2B). After the completion of vascular lineage induction, VI-BVOs not only expressed the vascular markers for endothelial cells (CD31) and pericytes (PDGFRβ) but also exhibited the ability of endothelial cells to take up ac-LDL (Figure 2C). Tube formation assays also showed that the endothelial cells in VI-BVOs exhibited angiogenic potential (Figure 2D). Flow cytometry revealed that 42.4% of the cells in VI-BVOs were CD 31$^+$ endothelial cells and 8.84% were CD 140b$^+$ pericytes at this stage (Figure 2E). Consistent with these findings, the qPCR results revealed that the expression of vascular-specific genes in VI-BVOs was significantly greater than that in ESCs (Figure 2F). To further explore the proliferation and differentiation of endothelial cells in VI-BVOs, we dissociated VI-BVOs into single cells and cultured the cells in 24-well plates for 3 days. A serial photographing of single cells to cell colonies exhibited proliferation ability of VI-BVOs-derived single cells (Figure 2G). The flow cytometry results showed that 44.3% of these cells were endothelial cells and 30.1% were pericytes (Figure 2H). Moreover, VI-BVOs-derived single cells included many CD31$^+$ endothelial cells (Figure 2I). These results show that VI-BVOs continue to proliferate and differentiate after dissociated into single cells and have characteristics similar to those of hydrogel-embedded BVOs. Based on the above experimental results, we determined that the differentiation characteristics of BVOs at different induction stages were similar to those observed during vasculogenesis and angiogenesis *in vivo*. Therefore, BVOs induction can be divided into two phases: vasculogenesis and angiogenesis.

Effects of high glucose on the mesoderm induction stage and vascular lineage induction stage of BVOs

Based on the above experimental results, we divided the induction process of BVOs into two phases, namely, vasculogenesis (comprising mesoderm induction and vascular lineage induction) and angiogenesis, an organization similar to the process of vascular development in human tissue (Figure 3A). To study the effect of high-glucose treatment on vasculogenesis in BVOs, we cultured ESC-EBs and MI-BVOs in high-glucose medium (75 mM glucose) for three consecutive days, with control medium (17 mM glucose +75mM D-mannitol) serving as the corresponding control environment. After high-glucose treatment for three days, the ESC-EBs were differentiated into MI-BVOs, and the MI-BVOs were differentiated into VI-BVOs. The immunofluorescence results showed that compared to MI-BVOs in the control (MI-Control) group, the expression of the mesodermal cell markers PDGFRα and FLK1 was significantly decreased in the high glucose (MI-HG) group (Figure 3B). The qPCR results were consistent with the immunofluorescence results, indicating that exposure to high-glucose conditions during the mesoderm induction stage can inhibit cell differentiation in MI-BVOs (Figure 3C). During the vascular induction stage, high-glucose medium (VI-HG group) can also inhibit the differentiation and function of vascular cells compared to control medium (VI-Control group), as indicated by the downregulating in the levels of the vascular markers CD31 and PDGFRβ; in addition, the uptake function of endothelial cells was inhibited (Figures 3D and S2). The qPCR results were consistent with the immunofluorescence results, indicating that exposure to high-glucose conditions during the vascular lineage induction stage can inhibit vascular cell differentiation in VI-BVOs (Figure 3E). The aforementioned findings

Figure 2. BVOs induction can be divided into two phases: Vasculogenesis and angiogenesis

(A) ESC-EBs are spread throughout OCT4+ and SSEA4+ ESCs.

(B) Compared with hucMSC-EBs, MI-BVOs had characteristics of mesoderm cells, both of which contained PDGFRα^+ and FLK1$^+$ mesodermal cells.

(C) VI-BVOs not only express vascular-related biomarkers for endothelial cells (CD31) and pericytes (PDGFRβ) but also have the functional characteristics of endothelial cells to take up Ac-LDL.

(D) The cells in VI-BVOs have angiogenic potential.

(E) In total, 42.4% of the cells in VI-BVOs were endothelial cells, and 8.84% were pericytes.

(F) qPCR revealed that the relevant gene expression levels in endothelial cells and pericytes were significantly greater than those in ESCs. Data are represented as mean ± SD. (n = 3 replicates per condition from 3 independent experiments, *p < 0.05, **p < 0.01, ***p < 0.001, ****p < 0.0001 from two-tailed Student's t test).

(G) Inverted phase contrast images showing that VI-BVOs-derived single cells can grow and multiply in planar culture.

(H) After 3 days of planar culture, 44.3% of the cells derived from VI-BVOs were endothelial cells, and 30.1% were pericytes.

(I) The VI-BVOs-derived single-cell population contained many CD31$^+$ endothelial cells. Scale bar: 100 μm.

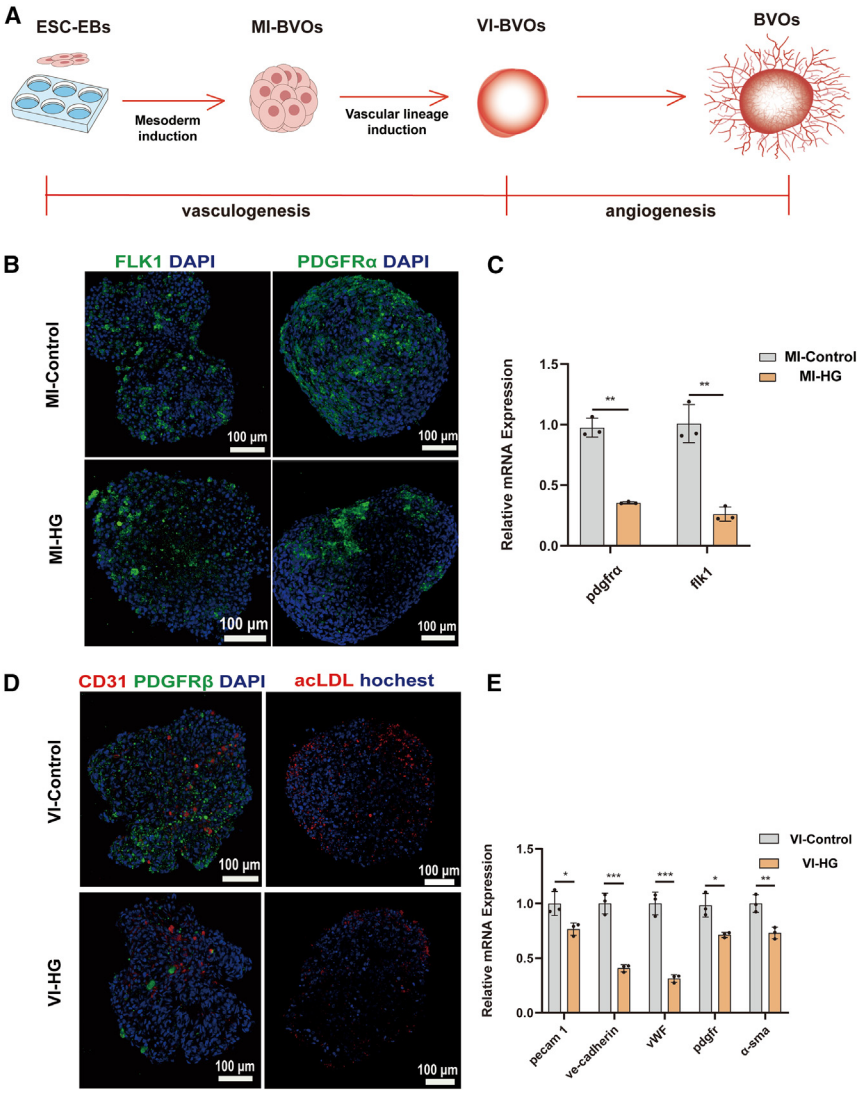

Figure 3. Effects of high glucose on the mesoderm induction stage and vascular lineage induction stage of BVOs

(A) Pattern diagrams for each stage of BVOs.

(B) Compared to the control treatment (MI-Control), high-glucose treatment (MI-HG) inhibited PDGFRα$^+$ and FLK1$^+$ mesodermal cell differentiation.

(C) qPCR analysis showed that high-glucose treatment inhibited pdgfrα/flk1 expression.

(D) Compared to the control treatment (VI-Control), high-glucose treatment (VI-HG) downregulated CD31$^+$ endothelial cells and PDGFRβ$^+$ pericytes differentiation levels, meanwhile inhibited the uptake function of endothelial cells.

(E) qPCR analysis showed that high-glucose treatment inhibited *Pecam1/VE-Cadherin/Pdgfr/α-Sma* gene expression. For (C) and (E), data are represented as mean ± SD. ($n = 3$ replicates per condition from 3 independent experiments, $^*p < 0.05$, $^{**}p < 0.01$, $^{***}p < 0.001$, $^{****}p < 0.0001$ from two-tailed Student's *t* test). Scale bar: 100 μm.

suggest that high-glucose treatment can inhibit the differentiation of cells in BVOs during the mesoderm and vascular lineage induction stages and these effects lead to abnormal vasculogenesis. Hence, we aimed to discern the stage at which high-glucose exposure exerts a more pronounced inhibitory impact on subsequent endothelial cell differentiation and function.

The vascular lineage induction stage is more sensitive to high-glucose treatment than the mesoderm induction stage of BVOs

In previous experiments, we found that high-glucose conditions can inhibit the differentiation and function of BVOs during both the mesoderm induction stage and the vascular lineage induction stage. To further discern the stage at which high-glucose exposure exerts a more pronounced inhibitory impact on subsequent endothelial cell differentiation and function, we cultured MI-BVOs to generate VI-BVOs that had been subjected to high-glucose treatment (75 mM glucose) for three days during the mesoderm induction stage (the MG group) compared with VI-BVOs that had been subjected to high-glucose treatment (75 mM glucose) for three days during the vascular induction stage (the VG group), and with VI-BVOs cultured in control medium (17 mM glucose +75mM D-mannitol) as the Control group. The immunofluorescence results showed that compared to VI-BVOs that in the Control group, the differentiation levels of and the ability to take up ac-LDL of CD31$^+$ endothelial cells were attenuated in the MG group and the VG group, meanwhile the VG group was inhibited more significantly than the MG group (Figures 4A and S3A). Flow cytometric analysis also confirmed that compared with that in the MG group (54.3%), the number of CD 31$^+$endothelial cells in the VG group (49.8%) was decreased, and both groups were inferior to the Control group (61.6%) (Figure 4B).Tube formation assays revealed that compared with that of the VI-BVOs in the Control group, the angiogenetic potential of the VI-BVOs in the MG group and the VG group was reduced, and then the VG group was poorer than the MG group (Figure 4C). When the VI-BVOs were embedded in the hydrogel, the sprouting of the VI-BVOs in the VG group and the MG group were attenuated compared with that in the Control group, and the VG group was poorer than the MG group (Figures 4D and S3B). In addition, the expression levels of endothelial cell markers and uptake function of endothelial cells in the Control group were highest and the VG group inferior to the MG group (Figure 4D), which showed that the effect of high glucose on VI-BVOs would influence the sprouting of BVOs. The qPCR results were consistent with the results of the above experiments, indicating that high-glucose treatment exhibits an increased inhibitory effect on the differentiation levels of VI-BVOs in the vascular lineage induction stage than in the mesoderm induction stage (Figure 4E). These results indicated that the vascular lineage

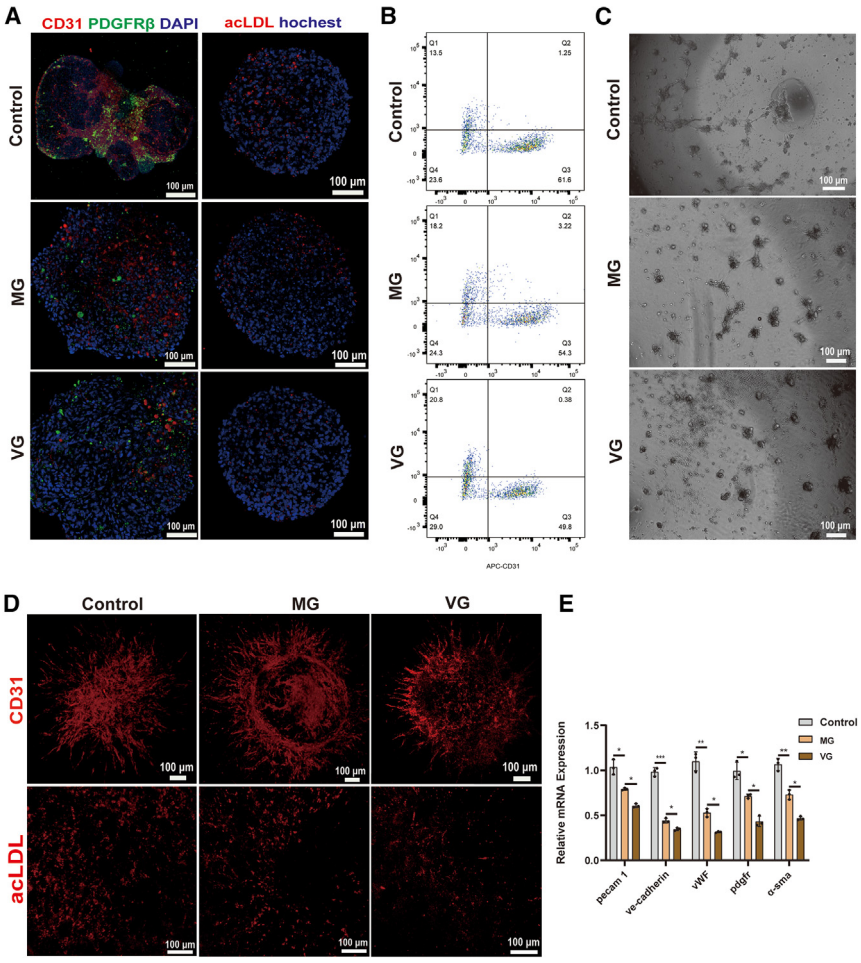

Figure 4. The vascular lineage induction stage is more sensitive to high-glucose treatment than the mesoderm induction stage of BVOs

(A) Control group: VI-BVOs in control medium (17 mM glucose +75mM D-mannitol); MG group: VI-BVOs treated with high-glucose medium in the mesoderm induction stage; VG group: VI-BVOs treated with high-glucose medium in the vascular lineage induction stage. The VG group showed poorer differentiation and function of endothelial cells than the MG group, both of which were inferior to the Control group.

(B) The VG group showed poorer angiogenetic potential than the MG group, both of which were inferior to Control group.

(C) The VG group (49.8%) had a lower percentage of endothelial cells than the MG group (54.3%), which both were inferior to Control group (61.6%).

(D) The sprouting of the VI-BVOs in the VG group and the MG group were attenuated compared with that in the Control group, and then the VG group was inhibited more significantly than the MG group.

(E) qPCR analysis showed that the VG group had a decreased gene expression levels of vascular cells compared with the MG group, both of which were inferior to the Control group. Data are represented as mean ± SD. ($n = 3$ replicates per condition from 3 independent experiments, $^{*}p < 0.05$, $^{**}p < 0.01$, $^{***}p < 0.001$, $^{****}p < 0.0001$ from one-way ANOVA). Scale bar: 100 μm.

induction stage was when BVOs were the most sensitive to high glucose levels. In subsequent experiments, we investigated the impact of hucMSCs on the growth and differentiation of BVOs exposed to high glucose conditions during the vascular lineage induction stage.

HucMSCs can alleviate abnormal vasculogenesis of VI-BVOs and subsequent angiogenesis of BVOs

To test whether hucMSCs can alleviate abnormal vasculogenesis caused by high-glucose conditions, we cocultured hucMSC-EBs and MI-BVOs at a ratio of 1:1 in high-glucose medium (75 mM glucose) for three consecutive days until the formation of VI-BVOs, with MI-BVOs cultured alone in high-glucose medium (75 mM glucose) and control medium (17 mM glucose +75mM D-mannitol) serving as the corresponding control. Under the coculture condition, both hucMSC-EBs and VI-BVOs exhibited a spherical morphology and robust growth. Some VI-BVOs and hucMSC-EBs self-aggregated into a merged EBs, and some remained free. Additionally, these structures were easily distinguished from a morphological perspective: hucMSC-EBs were more compact and less transparent, while VI-BVOs were more transparent (Figures 5A and S4). Subsequently, we selected free VI-BVOs from all groups for immunofluorescence staining, qPCR analysis and flow cytometric analysis. The immunofluorescence results showed that high glucose inhibited the differentiation and the ability to take up ac-LDL of endothelial cells. Meanwhile, the presence of hucMSC-EBs significantly improve the differentiation levels and function of endothelial cells (Figures 5B and S5A). Flow cytometric analysis also revealed that high glucose treatment decreased the proportion of endothelial cells and hucMSC-EBs can alleviate it (Figure 5C). The qPCR results were consistent with the above results, indicating that the expression levels of vascular-specific genes were significantly downregulated under high glucose treatment and the presence of hucMSC-EBs improve the phenomenon (Figure 5D). When the VI-BVOs were embedded in the hydrogel, the sprouting of the VI-BVOs in the MG group was poorer than the Control group but improved in the VG + hucMSCs group. (Figure 5E). In addition, the expression levels of CD 31 and the ac-LDL uptake function of endothelial cells in MG group were lower than the Control group but increased in the VG + hucMSCs group (Figures 5F and S5B).

hucMSCs can improve migration capabilities and proliferation levels of vascular cells derived from VI-BVOs

To further investigate the effects of hucMSCs on migration capabilities and proliferation levels of vascular cells derived from VI-BVOs, we dissociated the VI-BVOs from the Control group, VG group and VG + hucMSCs group into single cells and plated

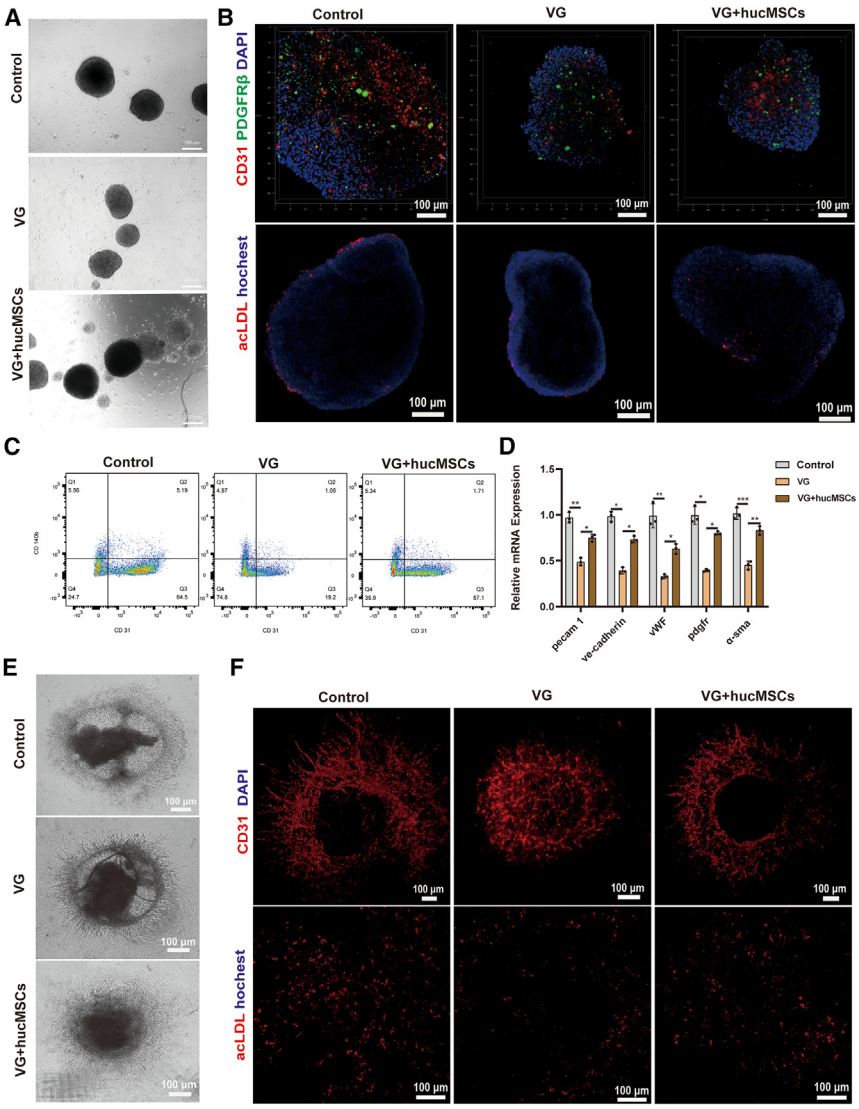

Figure 5. HucMSCs can alleviate abnormal vasculogenesis of VI-BVOs and subsequent angiogenesis of BVOs

(A) Inverted phase contrast images showed that the VI-BVOs had a spherical morphology and robust growth. Control group: MI-BVOs cultured alone in high-control medium for three consecutive days; VG group: MI-BVOs cultured alone in high-glucose medium for three consecutive days; VG + hucMSCs group: MI-BVOs and hucMSC-EBs cocultured in high-glucose medium for three consecutive days.

(B) The immunofluorescence results showing that high glucose inhibited the differentiation of endothelial cells and the ability to take up Ac-LDL, but hucMSCs alleviated the phenomenon.

(C) Flow cytometric analysis showed that high glucose lowered the proportion of endothelial cells, but hucMSCs alleviated the phenomenon.

(D) The qPCR results indicated that high glucose inhibited the expression levels of vascular-specific genes, and the presence of hucMSCs significantly improved the phenomenon. Data are represented as mean ± SD. ($n = 3$ replicates per condition from 3 independent experiments, $^{*}p < 0.05$, $^{**}p < 0.01$, $^{***}p < 0.001$, $^{****}p < 0.0001$ from one-way ANOVA).

(E) Inverted phase contrast images showed that high glucose inhibited the sprouting of VI-BVOs, and the presence of hucMSCs significantly improved the phenomenon.

(F) The immunofluorescence results showed that high glucose inhibited the expression levels of CD 31 and the uptake function of endothelial cells in BVOs, and the presence of hucMSCs significantly improved the phenomenon. Scale bar: 100 μm.

the cells in a 24-well plate following cultured them for 3 days. Flow cytometric analysis showed that high glucose decreased the proportion of endothelial cells, and the presence of hucMSCs improved the phenomenon, which was consistent with the above results (Figure 6A). MTT assay results showed that high glucose downregulated proliferation levels of vascular cells derived from VI-BVOs and hucMSCs treatment can alleviate the damage (Figure 6B). And the TUNEL assay results revealed that apoptosis levels were also increased in VG group compared to Control group (Figure 6C), but decreased in VG + hucMSCs group. Wound-healing assay also showed that high glucose treatment impaired the migration capabilities of vascular cells derived from VI-BVOs (Figure 6D) compared to control medium but improved in the presence of hucMSCs. The aforementioned results suggested that hucMSCs can not only ameliorate abnormal vasculogenesis induced by high glucose condition but also facilitate the proliferation levels and migration capabilities of vascular cells derived from VI-BVOs.

HucMSCs alleviate abnormal vasculogenesis in VI-BVOs caused by high-glucose treatment through the MAPK signaling pathway

It has been shown that hucMSCs can alleviate endothelial cell damage caused by high-glucose conditions through the MAPK signaling pathway[21]; thus, we investigated whether the effects of high glucose and hucMSCs on vasculogenic abnormalities are associated with the MAPK signaling pathway. To this end, we designed three sets of experiments with three groups: a control group (17 mM glucose), a VG group (75 mM glucose), and a VG + hucMSCs group (75 mM glucose). Flow cytometric analysis showed that high-glucose treatment significantly decreased the proportion of endothelial cells in VI-BVOs and that hucMSCs alleviated this effect (Figure 7A). Subsequently, we examined the expression levels of ERK/JNK/p38 and their phosphorylation related to the MAPK signaling pathway. High-glucose treatment significantly increased the phosphorylation levels of these proteins compared to those in the control group. After hucMSCs treatment, the phosphorylation levels of these proteins were decreased significantly (Figure 7B and 7C). To further confirm this observation, 100 μM MAPK activator Dimethyl fumarate (DMF, Sigma-Aldrich, St. Louis, MO, USA), known for significantly activated

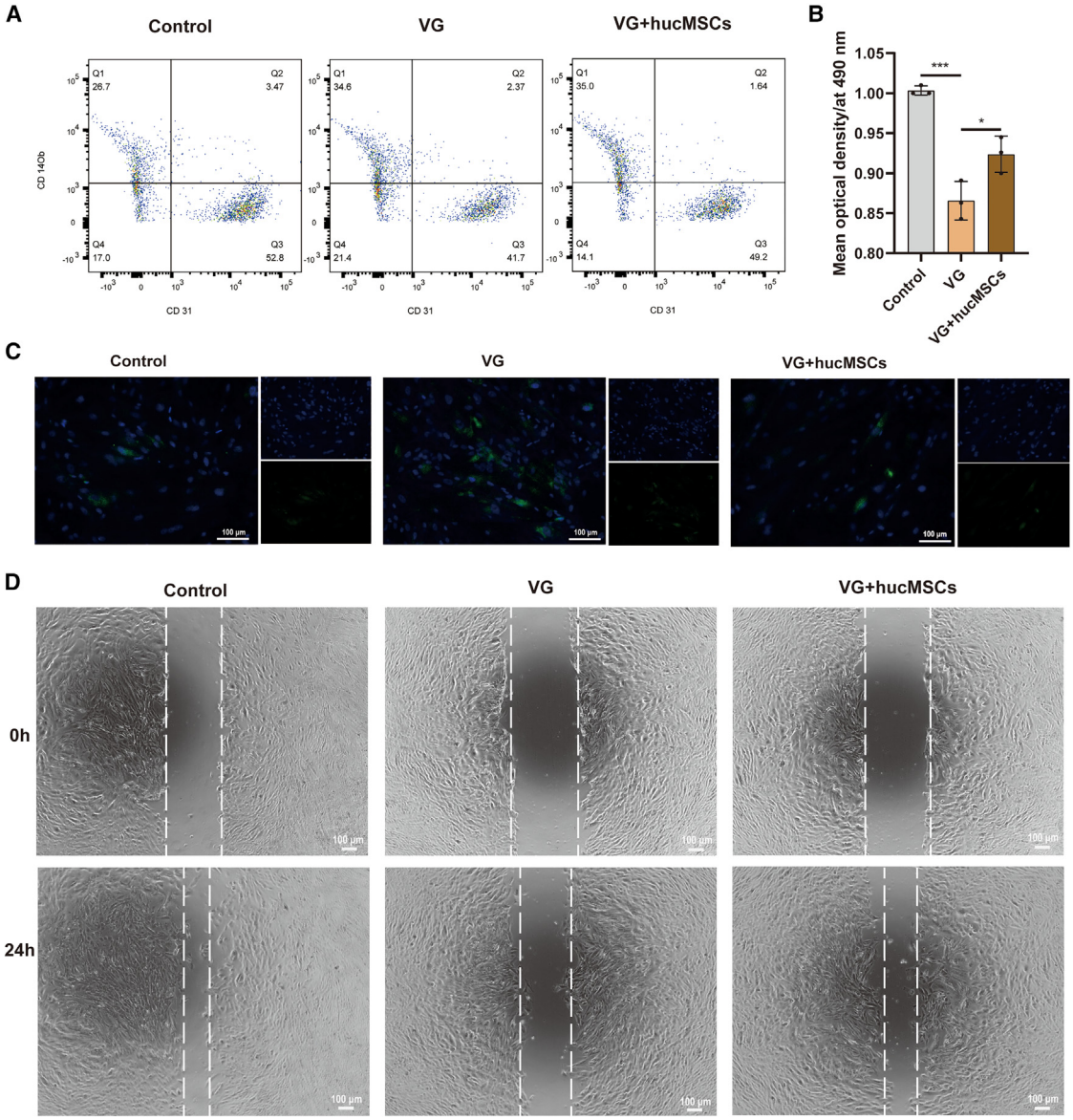

Figure 6. hucMSCs can improve migration capabilities and proliferation levels of vascular cells derived from VI-BVOs

(A) Flow cytometric analysis showed that high glucose treatment decreased the proportion of endothelial cells derived from VI-BVOs, and hucMSCs alleviated the phenomenon.

(B) MTT assay results showed high glucose inhibited the proliferation levels of vascular cells derived from VI-BVOs and hucMSCs treatment can improve the phenomenon. Data are represented as mean ± SD. (n = 3 replicates per condition from 3 independent experiments, *p < 0.05, **p < 0.01, ***p < 0.001, ****p < 0.0001 from one-way ANOVA).

(C) The TUNEL assay results showed that high glucose increased apoptosis levels of vascular cells derived from VI-BVOs, and hucMSCs can decrease apoptosis levels.

(D) Wound-healing assay showed that high glucose impaired the migration capabilities of vascular cells derived from VI-BVOs and hucMSCs treatment improved the phenomenon. Scale bar: 100 μm.

JNK/p38/ERK,[22] were added into the co-culture system (VG+hucMSCs+DMF group). The addition of MAPK activators increased the proportion of endothelial cells in VG+hucMSCs+DMF group compared to VG + hucMSCs group, meanwhile resulted in the upregulation of the phosphorylation levels of ERK/JNK/p38 (Figure 7D–7F). Hence, we concluded that hucMSCs alleviate the impairment of endothelial cell in VI-BVOs caused by high-glucose treatment during the vascular lineage induction stage through the MAPK signaling pathway.

DISCUSSION

The cardiovascular system is the first functional system to arise during human embryonic development, becoming active

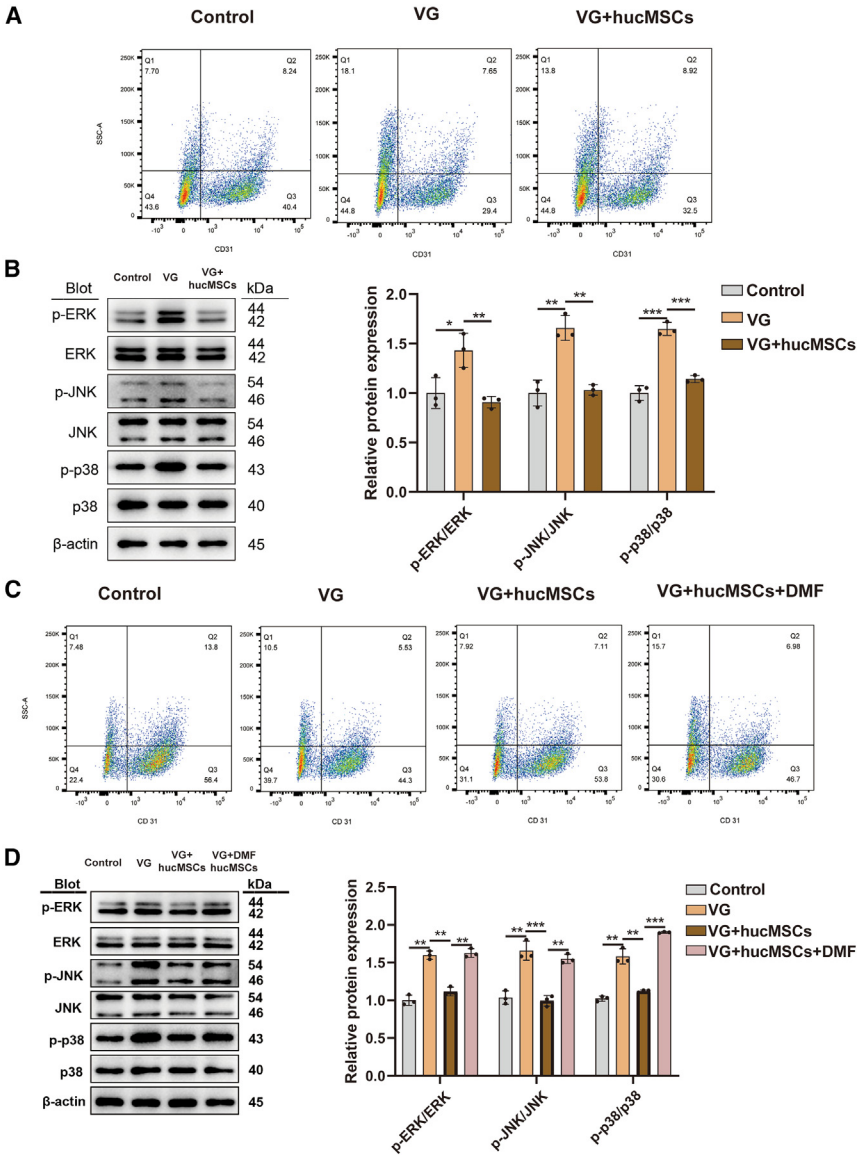

Figure 7. HucMSCs alleviate abnormal vasculogenesis in VI-BVOs caused by high-glucose treatment through the MAPK signaling pathway

(A) Flow cytometric analysis showed that high-glucose treatment decreased the proportion of endothelial cells and that coculturing with hucMSCs alleviated this effect.

(B) The Western blot results showed that high-glucose treatment increased the phosphorylation levels of ERK/JNK/p38 compared to those in the control group, but hucMSCs treatment decreased the phosphorylation levels of these proteins.

(C) Flow cytometric analysis showed that MAPK activator treatment increased the proportion of endothelial cells in VG+hucMSCs+DMF group compared to VG + hucMSCs group.

(D) The Western blot results showed that MAPK activator treatment increased the phosphorylation levels of ERK/JNK/p38 compared to those in the VG + hucMSCs group. For (B) and (D), data are represented as mean ± SD. (n = 3 replicates per condition from 3 independent experiments, $^{*}p < 0.05$, $^{**}p < 0.01$, $^{***}p < 0.001$, $^{****}p < 0.0001$ from one-way ANOVA). Scale bar: 100 μm.

at approximately the third to fourth week of gestation.[23] The formation of blood vessels and subsequent blood flow ensure the survival and development of the embryo.[11,23] The developing tissue is permeated and interconnected by an intricate network of vascular systems, facilitating not only the exchange of oxygen, nutrients, and metabolic waste but also contributing to the structural formation of tissues and organs.[23,24] Vascular injuries can lead to a range of diseases. In patients with diabetes, endothelial cell damage and vascular complications caused by high glucose levels are the primary factors leading to disability and the incidence of diabetes.[25] Therefore, for the repair of damaged blood vessels and the treatment of vascular complications, the main strategies are controlling blood glucose, improving endothelial cell function and promoting endothelial cell proliferation and migration.

During the development of human blood vessels, vasculogenesis, which refers to the *de novo* generation of endothelial cells from endothelial progenitor cells (EPCs).[8,14] As the first step in the vascular system, vasculogenesis determines the degree of differentiation of endothelial cells, which plays a very important role in the formation and repair of blood vessels. Abnormalities in vasculogenesis inevitably result in abnormalities in the vascular system. Researchers have shown that during *in vitro* culture of mouse embryos, abnormalities in vasculogenesis can lead to abnormal embryonic development or even malformations. Moreover, vasculogenesis also occurs in adult tissues and involved in the formation of vascular system and the repair of damaged blood vessel. For example, EPC-EXs can protect against high glucose-derived endothelial cell damage and cerebral ischemic injury by improving astrocyte survival and oxidative stress.[26] EPCs can also serve as biomarkers of cardiovascular risk.[15] However, to date, studies on diabetes mellitus have overlooked the importance of vasculogenesis and research on vasculogenesis is limited.

BVOs are generated from ESCs or PSCs that have undergone mesodermal induction and vascular lineage induction stage *in vitro* and then are embedded in a gel.[17] By an in-depth study of BVOs, we found that the induction process of BVOs is very similar to process of human blood vessel development, both of which demonstrated that endothelial cells are originated from flk1-positive mesodermal progenitor cells.[27,28] Therefore, BVOs serve as an excellent *in vitro* platform for the study the

effect of high glucose on vasculogenesis and the specific mechanism.

In this study, we first characterized the various induction stages of BVOs and found that the mesodermal induction stage and the vascular induction stage were highly similar to vasculogenesis. Subsequently, to explore the impact of high glucose on mesodermal cells differentiation and subsequent vascular cells differentiation of BVOs, we treated BVOs at each of induction stages with high-glucose (75 mM) medium. Strictly speaking, the glucose concentration of 75 mM is super-physiological, which is 2–3 times the level seen in diabetic patients with hyperglycemic hyperosmolar syndrome (HHS).[29] And ISPAD Clinical Practice Consensus Guidelines 2018 defined that the average fasting blood glucose (FBG) concentration exceeding 145 mg/dL (8mM) is deemed as poor glycemic control,[30,31] which is the essential cardiovascular disease risk factors.[32] However, from the perspective of *in vitro* experiments, the choice of 75mM concentration was a comprehensive decision based on literature references and experimental findings. In two-dimensional endothelial cell models, the glucose concentrations generally fall between 30 and 50 mM,[33,34] and in some studies exploring endothelial-mesenchymal transition, the glucose concentrations even reach 100 mM.[35] In the diabetic model of BVOs, the glucose concentration is set at 75 mM.[16] Therefore, based on literature research, we preliminarily investigated the effects of 35 mM and 75 mM glucose on BVOs. The experimental results indicated that both 35 mM and 75 mM glucose could individually inhibit cells differentiation levels in MI-BVOs and VI-BVOs. However, when we transferred high glucose-treated MI-BVOs to a non-high glucose medium for further induction into VI-BVOs and examined the effects of high glucose on subsequent endothelial cell differentiation, we observed that 35 mM glucose treatment to MI-BVOs did not accurately predict the endothelial cells differentiation inhibition during the subsequent vascular lineage induction stage. Only 75 mM glucose could reliably capture this outcome. This may result from the fact that damage to MI-BVOs from glucose of lower concentrations remains within the cellular compensation range, potentially repairable during subsequent vascular lineage induction stage. Whereas glucose of high concentrations can disrupt this compensatory mechanism. Therefore, in order to ensure the reproducibility of the experiment, we chose 75mM glucose for further research. Based on this, to determine the induction stage of BVOs at which high-glucose treatment has the greatest impact on the differentiation and function of endothelial cells, we compared endothelial cell differentiation levels of VI-BVOs after high glucose treatment during the mesoderm stage and the vascular lineage induction stage, respectively. And we found that the vascular lineage induction stage was most susceptible to the effects of high glucose. Therefore, our next experiments focused on high-glucose treatment at the vascular lineage induction stage.

Currently, stem cell therapies targeting endothelial cells and angiogenesis are widely researched.[36] Many clinical and experimental studies have demonstrated that hucMSCs can alleviate the symptoms of patients with diabetes, reduce endothelial cell damage, and regulate angiogenesis to alleviate vascular complications of diabetes.[37–39] Additionally, mesenchymal stem cells, which are stem cells originating from the mesoderm, not only facilitate the differentiation of endothelial cells via paracrine signaling, but also possess the capability to differentiate into endothelial cells themselves.[40,41] Therefore, we considered whether cocultures between BVOs and hucMSCs can improve abnormal vasculogenesis.

During the experiment, we discovered that hucMSCs exhibit a strong capability for self-aggregation and it can self-aggregate into EBs under suspension culture conditions; these EBs are more compact than those formed by ESCs, and they exhibit robust growth under coculture conditions.[42,43] Through analysis the differentiation levels, proliferation levels and migration capability of VI-BVOs and vascular cells derived from VI-BVOs after coculture, we found that hucMSCs indeed alleviated the abnormal differentiation of mesodermal cells and subsequent sets of endothelial cells resulting from high-glucose treatment. Preliminary research had shown that hucMSCs can alleviate endothelial cell damage through the MAPK signaling pathway.[21] And we thus investigated whether hucMSCs can alleviate the abnormal differentiation of endothelial cells through this pathway.[21] To this end, we examined the expression of relevant markers of this signaling pathway with the addition of MAPK activator DMF and found that the MARK signaling pathway is indeed involved in the regulation of endothelial cell differentiation.

In this study, we skillfully exploited the different induction stages of BVOs, and through an in-depth analysis of BVOs, we found that the induction of BVOs *in vitro* involves a process similar to that of vascular development in humans. Based on this concept, other organoid generated from ESCs/PSCs could be used for research of corresponding tissues development.

Limitations of the study

Although this platform was used in this study to explore the vascular differentiation process, this study still has limitations. First, the inhibitory effect of high glucose on endothelial cell differentiation is supposed to be slow and persistent. However, the fixed strategy employed in the BVOs induction protocol somewhat restricts our ability to subject BVOs to longer periods using lower concentrations of glucose. This may also be one of the reasons why the glucose concentration *in vitro* must be maintained in super-physiological levels. Second, vascular cell differentiation is carried out at the embryonic level, but individual BVOs lack interaction with other tissues and organs can only mimic the influence of a single cell lineage.[44] Therefore, in future studies, we can consider the use of stem cell–derived embryonic organoids for mutual validation at the organoid and embryo levels. This approach may be highly important for obtaining an in-depth understanding of the mechanism underlying embryonic vascular development and furthering the treatment of diabetic vascular diseases.

RESOURCE AVAILABILITY

Lead contact

Further information and requests for reagents may be directed to, and will be fulfilled upon reasonable request by, the lead contact X.L. (yingbaby1010@163.com).

Materials availability

This study did not generate new unique reagents. The used drugs were purchased from commercial vendors as stated in the key resources table.

Data and code availability

- The datasets generated and analyzed related to this paper are available from the lead contact on reasonable request.
- This paper does not report original code.
- Any additional information required to reanalyze the data reported in this paper is available from the lead contact upon request.

ACKNOWLEDGMENTS

We thank all our authors listed in this manuscript. This work was supported by the Evergreen tree Excellent Young and middle-aged Doctors Training Project of Central Hospital Affiliated to Shandong First Medical University (TJJH2021003).

AUTHOR CONTRIBUTIONS

Conceptualization, Y.Y. and X.L.; methodology, Y.Y. and X.L.; formal analysis, Y.Y. and T.S.; investigation, Y.Y., T.S., and X.L.; writing – original draft, Y.Y. and X.L.; visualization, Y.Y.; supervision, X.L.; funding acquisition, X.L.

DECLARATION OF INTERESTS

The authors declare no competing interests.

STAR★METHODS

Detailed methods are provided in the online version of this paper and include the following:

- KEY RESOURCES TABLE
- EXPERIMENTAL MODEL AND STUDY PARTICIPANT DETAILS
  - hESCs culture
  - hucMSCs culture
  - Generation of hESC-derived BVOs
  - Establishment of a high-glucose model for BVOs
  - Coculture of hucMSC-derived EBs and ESC-derived VI-BVOs
- METHOD DETAILS
  - Whole-mount immunofluorescence staining
  - Acetylated low-density lipoprotein (AcLDL) uptake assay
  - Hematoxylin-eosin (HE) staining
  - Flow cytometry
  - Matrigel tube formation assay
  - Wound-Healing Assay
  - Terminal deoxynucleotidyl transferase dUTP nick end labeling (TUNEL) assay
  - 3-(4,5-Dimethylthiazol-2-yl)-2,5-diphenyl tetrazolium bromide (MTT) assay
  - Quantitative PCR (qPCR)
  - Western blot analysis
- QUANTIFICATION AND STATISTICAL ANALYSIS

SUPPLEMENTAL INFORMATION

Supplemental information can be found online at https://doi.org/10.1016/j.isci.2024.111354.

Received: June 17, 2024
Revised: August 27, 2024
Accepted: November 6, 2024
Published: November 9, 2024

REFERENCES

1. Sun, H., Saeedi, P., Karuranga, S., Pinkepank, M., Ogurtsova, K., Duncan, B.B., Stein, C., Basit, A., Chan, J.C.N., Mbanya, J.C., et al. (2022). IDF Diabetes Atlas: Global, regional and country-level diabetes prevalence estimates for 2021 and projections for 2045. Diabetes Res. Clin. Pract. *183*, 109119.
2. Cole, J.B., and Florez, J.C. (2020). Genetics of diabetes mellitus and diabetes complications. Nat. Rev. Nephrol. *16*, 377–390.
3. Dubsky, M., Veleba, J., Sojakova, D., Marhefkova, N., Fejfarova, V., and Jude, E.B. (2023). Endothelial Dysfunction in Diabetes Mellitus: New Insights. Int. J. Mol. Sci. *24*, 10705.
4. Xu, S., Ilyas, I., Little, P.J., Li, H., Kamato, D., Zheng, X., Luo, S., Li, Z., Liu, P., Han, J., et al. (2021). Endothelial Dysfunction in Atherosclerotic Cardiovascular Diseases and Beyond: From Mechanism to Pharmacotherapies. Pharmacol. Rev. *73*, 924–967.
5. Stanhewicz, A.E., Wenner, M.M., and Stachenfeld, N.S. (2018). Sex differences in endothelial function important to vascular health and overall cardiovascular disease risk across the lifespan. Am. J. Physiol. Heart Circ. Physiol. *315*, H1569–H1588.
6. Shi, Y., and Vanhoutte, P.M. (2017). Macro- and microvascular endothelial dysfunction in diabetes. J. Diabetes *9*, 434–449.
7. Li, Y., Liu, Z., Han, X., Liang, F., Zhang, Q., Huang, X., Shi, X., Huo, H., Han, M., Liu, X., et al. (2024). Dynamics of Endothelial Cell Generation and Turnover in Arteries During Homeostasis and Diseases. Circulation *149*, 135–154.
8. Payne, S., Neal, A., and De Val, S. (2024). Transcription factors regulating vasculogenesis and angiogenesis. Dev. Dyn. *253*, 28–58.
9. Boucher, D.M., and Pedersen, R.A. (1996). Induction and differentiation of extra-embryonic mesoderm in the mouse. Reprod. Fertil. Dev. *8*, 765–777.
10. Moccia, F., Negri, S., Shekha, M., Faris, P., and Guerra, G. (2019). Endothelial Ca(2+) Signaling, Angiogenesis and Vasculogenesis: just What It Takes to Make a Blood Vessel. Int. J. Mol. Sci. *20*, 3962.
11. Dong, D., Reece, E.A., Lin, X., Wu, Y., AriasVillela, N., and Yang, P. (2016). New development of the yolk sac theory in diabetic embryopathy: molecular mechanism and link to structural birth defects. Am. J. Obstet. Gynecol. *214*, 192–202.
12. Yang, P., and Reece, E.A. (2011). Role of HIF-1α in maternal hyperglycemia-induced embryonic vasculopathy. Am. J. Obstet. Gynecol. *204*, 332.e1–332.e7.
13. Weng, H., Li, X., Reece, E.A., and Yang, P. (2012). SOD1 suppresses maternal hyperglycemia-increased iNOS expression and consequent nitrosative stress in diabetic embryopathy. Am. J. Obstet. Gynecol. *206*, 448.e1–448.e7.
14. Nath, A.K., Enciso, J., Kuniyasu, M., Hao, X.Y., Madri, J.A., and Pinter, E. (2004). Nitric oxide modulates murine yolk sac vasculogenesis and rescues glucose induced vasculopathy. Development *131*, 2485–2496.
15. Ratajska, A., Jankowska-Steifer, E., Czarnowska, E., Olkowski, R., Gula, G., Niderla-Bielińska, J., Flaht-Zabost, A., and Jasińska, A. (2017). Vasculogenesis and Its Cellular Therapeutic Applications. Cells Tissues Organs *203*, 141–152.
16. Wimmer, R.A., Leopoldi, A., Aichinger, M., Wick, N., Hantusch, B., Novatchkova, M., Taubenschmid, J., Hämmerle, M., Esk, C., Bagley, J.A., et al. (2019). Human blood vessel organoids as a model of diabetic vasculopathy. Nature *565*, 505–510.
17. Wimmer, R.A., Leopoldi, A., Aichinger, M., Kerjaschki, D., and Penninger, J.M. (2019). Generation of blood vessel organoids from human pluripotent stem cells. Nat. Protoc. *14*, 3082–3100.
18. Zakrzewski, W., Dobrzyński, M., Szymonowicz, M., and Rybak, Z. (2019). Stem cells: past, present, and future. Stem Cell Res. Ther. *10*, 68.
19. Caplan, A.I., and Correa, D. (2011). The MSC: an injury drugstore. Cell Stem Cell *9*, 11–15.

20. Hu, J., Yu, X., Wang, Z., Wang, F., Wang, L., Gao, H., Chen, Y., Zhao, W., Jia, Z., Yan, S., and Wang, Y. (2013). Long term effects of the implantation of Wharton's jelly-derived mesenchymal stem cells from the umbilical cord for newly-onset type 1 diabetes mellitus. Endocr. J. *60*, 347–357.

21. Liu, Y., Chen, J., Liang, H., Cai, Y., Li, X., Yan, L., Zhou, L., Shan, L., and Wang, H. (2022). Human umbilical cord-derived mesenchymal stem cells not only ameliorate blood glucose but also protect vascular endothelium from diabetic damage through a paracrine mechanism mediated by MAPK/ERK signaling. Stem Cell Res. Ther. *13*, 258.

22. Xie, X., Zhao, Y., Ma, C.Y., Xu, X.M., Zhang, Y.Q., Wang, C.G., Jin, J., Shen, X., Gao, J.L., Li, N., et al. (2015). Dimethyl fumarate induces necroptosis in colon cancer cells through GSH depletion/ROS increase/MAPKs activation pathway. Br. J. Pharmacol. *172*, 3929–3943.

23. Vargas-Valderrama, A., Messina, A., Mitjavila-Garcia, M.T., and Guenou, H. (2020). The endothelium, a key actor in organ development and hPSC-derived organoid vascularization. J. Biomed. Sci. *27*, 67.

24. Zhang, S., Wan, Z., and Kamm, R.D. (2021). Vascularized organoids on a chip: strategies for engineering organoids with functional vasculature. Lab Chip *21*, 473–488.

25. Harding, J.L., Pavkov, M.E., Magliano, D.J., Shaw, J.E., and Gregg, E.W. (2019). Global trends in diabetes complications: a review of current evidence. Diabetologia *62*, 3–16.

26. Halurkar, M.S., Wang, J., Chen, S., and Bihl, J.C. (2022). EPC-EXs improve astrocyte survival and oxidative stress through different uptaking pathways in diabetic hypoxia condition. Stem Cell Res. Ther. *13*, 91.

27. Kataoka, H., Hayashi, M., Nakagawa, R., Tanaka, Y., Izumi, N., Nishikawa, S., Jakt, M.L., Tarui, H., and Nishikawa, S.I. (2011). Etv2/ER71 induces vascular mesoderm from Flk1+PDGFRα+ primitive mesoderm. Blood *118*, 6975–6986.

28. Yamashita, J., Itoh, H., Hirashima, M., Ogawa, M., Nishikawa, S., Yurugi, T., Naito, M., Nakao, K., and Nishikawa, S. (2000). Flk1-positive cells derived from embryonic stem cells serve as vascular progenitors. Nature *408*, 92–96.

29. Umpierrez, G.E., Davis, G.M., ElSayed, N.A., Fadini, G.P., Galindo, R.J., Hirsch, I.B., Klonoff, D.C., McCoy, R.G., Misra, S., Gabbay, R.A., et al. (2024). Hyperglycaemic crises in adults with diabetes: a consensus report. Diabetologia *67*, 1455–1479.

30. Habteyohans, B.D., Hailu, B.S., Meseret, F., Mohammed, A., Berhanu, Y., Alemu, A., Tolosa, G., Keneni, M., and Desalew, A. (2023). Poor glycemic control and its associated factors among children with type 1 diabetes mellitus in Harar, eastern Ethiopia: A cross-sectional study. BMC Endocr. Disord. *23*, 208.

31. Mayer-Davis, E.J., Kahkoska, A.R., Jefferies, C., Dabelea, D., Balde, N., Gong, C.X., Aschner, P., and Craig, M.E. (2018). ISPAD Clinical Practice Consensus Guidelines 2018: Definition, epidemiology, and classification of diabetes in children and adolescents. Pediatr. Diabetes *19*, 7–19.

32. Khanal, M.K., Bhandari, P., Dhungana, R.R., Gurung, Y., Rawal, L.B., Pandey, G., Bhandari, M., Devkota, S., Courten, M.d., and Courten, B.d. (2022). Poor glycemic control, cardiovascular disease risk factors and their clustering among patients with type 2 diabetes mellitus: A cross-sectional study from Nepal. PLoS One *17*, e0271888.

33. Zhang, Y., Xi, X., Mei, Y., Zhao, X., Zhou, L., Ma, M., Liu, S., Zha, X., and Yang, Y. (2019). High-glucose induces retinal pigment epithelium mitochondrial pathways of apoptosis and inhibits mitophagy by regulating ROS/PINK1/Parkin signal pathway. Biomed. Pharmacother. *111*, 1315–1325.

34. Li, Q., Wen, Y., Wang, L., Chen, B., Chen, J., Wang, H., and Chen, L. (2021). Hyperglycemia-induced accumulation of advanced glycosylation end products in fibroblast-like synoviocytes promotes knee osteoarthritis. Exp. Mol. Med. *53*, 1735–1747.

35. Yu, C.H., Suriguga, Gong, M., Liu, W.J., Cui, N.X., Wang, Y., Du, X., and Yi, Z.C. (2017). High glucose induced endothelial to mesenchymal transition in human umbilical vein endothelial cell. Exp. Mol. Pathol. *102*, 377–383.

36. Päth, G., Perakakis, N., Mantzoros, C.S., and Seufert, J. (2019). Stem cells in the treatment of diabetes mellitus - Focus on mesenchymal stem cells. Metabolism *90*, 1–15.

37. Fiori, A., Terlizzi, V., Kremer, H., Gebauer, J., Hammes, H.P., Harmsen, M.C., and Bieback, K. (2018). Mesenchymal stromal/stem cells as potential therapy in diabetic retinopathy. Immunobiology *223*, 729–743.

38. Nagaishi, K., Mizue, Y., Chikenji, T., Otani, M., Nakano, M., Konari, N., and Fujimiya, M. (2016). Mesenchymal stem cell therapy ameliorates diabetic nephropathy via the paracrine effect of renal trophic factors including exosomes. Sci. Rep. *6*, 34842.

39. Cao, Y., Gang, X., Sun, C., and Wang, G. (2017). Mesenchymal Stem Cells Improve Healing of Diabetic Foot Ulcer. J. Diabetes Res. *2017*, 9328347.

40. Pham, T.X.A., Panda, A., Kagawa, H., To, S.K., Ertekin, C., Georgolopoulos, G., van Knippenberg, S.S.F.A., Allsop, R.N., Bruneau, A., Chui, J.S.H., et al. (2022). Modeling human extraembryonic mesoderm cells using naive pluripotent stem cells. Cell Stem Cell *29*, 1346–1365.e10.

41. Wang, C., Li, Y., Yang, M., Zou, Y., Liu, H., Liang, Z., Yin, Y., Niu, G., Yan, Z., and Zhang, B. (2018). Efficient Differentiation of Bone Marrow Mesenchymal Stem Cells into Endothelial Cells in Vitro. Eur. J. Vasc. Endovasc. Surg. *55*, 257–265.

42. Takebe, T., Sekine, K., Enomura, M., Koike, H., Kimura, M., Ogaeri, T., Zhang, R.R., Ueno, Y., Zheng, Y.W., Koike, N., et al. (2013). Vascularized and functional human liver from an iPSC-derived organ bud transplant. Nature *499*, 481–484.

43. Takebe, T., Zhang, R.R., Koike, H., Kimura, M., Yoshizawa, E., Enomura, M., Koike, N., Sekine, K., and Taniguchi, H. (2014). Generation of a vascularized and functional human liver from an iPSC-derived organ bud transplant. Nat. Protoc. *9*, 396–409.

44. Weatherbee, B.A.T., Gantner, C.W., Iwamoto-Stohl, L.K., Daza, R.M., Hamazaki, N., Shendure, J., and Zernicka-Goetz, M. (2023). Pluripotent stem cell-derived model of the post-implantation human embryo. Nature *622*, 584–593.

STAR★METHODS

KEY RESOURCES TABLE

REAGENT or RESOURCE	SOURCE	IDENTIFIER
Antibodies		
Alexa Fluor® 647 Mouse anti-Human CD31	BD Pharmingen™	Cat# 558094; RRID:AB_397020
PDGF Receptor β (28E1) Rabbit mAb	Cell Signaling	Cat# 3169S; RRID:AB_2162497
COL4A2-specific Polyclonal antibody	Proteintech	Cat# 55131-1-AP; RRID:AB_2881273
Oct-4 Antibody	Cell Signaling	Cat# 2750; RRID:AB_823583
SSEA-4 antibody	Santa Cruz Biotechnology	Cat#sc-59368; RRID:AB_1129653
Anti-PDGFR alpha Antibody	Abcam	Cat#ab203491; RRID:AB_2892065
VEGF Receptor 2 Recombinant Rabbit Monoclonal Antibody	HUABIO	Cat#ET1608-33; RRID:AB_3069801
p44/42 MAPK (Erk1/2) (137F5) Rabbit mAb	Cell Signaling	Cat#4695; RRID:AB_390779
Phospho-p44/42 MAPK (Erk1/2) (Thr202/Tyr204) (D13.14.4E) XP® Rabbit mAb	Cell Signaling	Cat#4370; RRID:AB_2315112
SAPK/JNK Antibody	Cell Signaling	Cat#9252; RRID:AB_2250373
Phospho-SAPK/JNK (Thr183/Tyr185) (81E11) Rabbit mAb	Cell Signaling	Cat#4668; RRID:AB_823588
p38 MAPK (D13E1) XP® Rabbit mAb	Cell Signaling	Cat#8690; RRID:AB_10999090
Phospho-p38 MAPK (Thr180/Tyr182) (D3F9) XP® Rabbit mAb	Cell Signaling	Cat#4511; RRID:AB_2139682
PE-conjugated mouse anti-human CD140b antibody	BD Pharmingen™	Cat#558821; RRID:AB_397132
Chemicals, peptides, and recombinant proteins		
Fetal bovine serum	ScienCell Research Laboratory	Cat#0510
mTeSR™ Plus Basal Medium	Stem Cell Technologies	Cat#100-0276
Matrigel	Corning	Cat#354230
penicillin–streptomycin	Gibco	Cat#15140122
nonessential amino acids	Sigma–Aldrich	Cat#M7145
Gentle Cell Dissociation Reagent	Stem Cell Technologies	Cat#100-0485
Y27632	Stem Cell Technologies	Cat#72304
Neurobasal™ Medium	Gibco	Cat#21103049
N-2 Supplement	Gibco	Cat#17502048
B-27™ Supplement	Gibco	Cat#17504044
GlutaMAX™ Supplement	Gibco	Cat#35050061
2-Mercaptoethanol	Gibco	Cat#21985023
CHIR-99021	APExBIO	Cat#A3011
Human BMP-4 Recombinant Protein	PeproTech	Cat#120-05
HumanKine® recombinant human VEGF165 protein- GMP grade	Proteintech	Cat#HZ-1038
forskolin	Sigma-Aldrich	Cat#F3917
Collagen I	Gibco	Cat#A1048301
StemPro™-34 SFM (1X)	Gibco	Cat#10639011
Recombinant Human FGF-basic	PeproTech	Cat#100-18B
bovine serum albumin	Solarbio	Cat#A8020
DiI AcLDL solution	Invitrogen	Cat#L3484
Collagenase B	Gibco	Cat#17101015
Trizol reagent	Ambion Life Technologies	Cat#15596018CN
PVDF Membrane	MIllipore	Cat# IPVH00010

(*Continued on next page*)

Continued

REAGENT or RESOURCE	SOURCE	IDENTIFIER
3-(4,5-Dimethylthiazol-2-yl)-2,5-diphenyl tetrazolium bromide	Invitrogen	Cat# M6494
Dimethyl sulfoxide	Thermo Scientific	Cat# 20688
Native lysis buffer	Abcam	Cat#ab156035
Critical commercial assays		
TB Green Premix Ex Taq II kit	TaKaRa	Cat# RR820A
PrimeScript RT Reagent Kit	TaKaRa	Cat# RR047A
TUNEL Apoptosis Assay Kit (Green Fluorescence)	TaKaRa	Cat# KTA2010
Experimental models: Cell lines		
H9 human Embryonic Stem Cells	ATCC	N/A
Human umbilical cord-derived mesenchymal stem cells	Procell	N/A
Oligonucleotides		
Primer: hPECAM1-F (AGACGTGCAGTACACGGAAG) and hPECAM1-R (TTTCCACGGCATCAGGGAC)	TaKaRa	N/A
Primer: *hVE-Cadherin* -F (*CGCAATAGACAAGGA CATAACAC*) and *hVE-Cadherin* -R (*GGTCAAA CTGCCCATACTTG*)	TaKaRa	N/A
Primer: *h-VWF* -F (*TCCACAAAACAATGAGT TCCAACT*) and *h-VWF* -R (*CCTGAACAA GTGTTTTCCAGTCTGT*)	TaKaRa	N/A
Primer: *hPDGFR* -F (*ATCAGCAGCAAGGCGAGC*) and *hPDGFR* -R (*CAGGTCAGAACGAAGGTGCT*)	TaKaRa	N/A
Primer: α-*SMA* -F (*GTGACTACTGCCGAGCGTG*) and α-*SMA* -R (*ATAGGTGGTTTCGTGGATGC*)	TaKaRa	N/A
Primer: *hCol4a1*-F (*TGCTGTTGAAAGGTGAAAGAG*) and *hCol4a1*-R (*CTTGGTGGCGAAGTCTCC*)	TaKaRa	N/A
Primer: *hCol4a2*-F (*ACAGCAAGGCAACAGAGG*) and *hCol4a2*-R (*GAGTAGGCAGGTAGTCCAG*)	TaKaRa	N/A
Primer: *PDGFR*α -F (*GCGGCCGCATGGGG ACTTCCCATCC*) and *PDGFR*α-R (*CTCGA GCAGGAAGCTGTCTTCCACC*)	TaKaRa	N/A
Primer: *FLK1*-F (*GAGGGGAACTGAAGACAGGC*) and *FLK1*-R (*GGCCAAGAGGCTTACCTAGC*)	TaKaRa	N/A
Primer: *hGAPDH* -F (*GCTTCCGTGGACACATAAC*) and *hGAPDH* -R (*TGGTGCCTTCTCCCTTC*)	TaKaRa	N/A
Software and algorithms		
ImageJ	National Institutes of Health	https://mirror.imagej.net
GraphPad Prism (version 9.3.1)	GraphPad Software	https://www.graphpad.com
FlowJo v10.8.1	BD Biosciences	https://www.flowjo.com/

EXPERIMENTAL MODEL AND STUDY PARTICIPANT DETAILS

hESCs culture

H9 human ESCs (hESCs; WA09/H9; ATCC, USA) were maintained in mTeSR Plus Basal Medium (Stem Cell Technologies, 100–0276, CA, USA) in Matrigel (Corning, Kennebunk, ME, USA)-coated 6-well culture plates. The medium was replaced every day, and the cells were passaged routinely when they reached 80% confluence.

hucMSCs culture

hucMSCs (Procell, Wuhan, China) were maintained in DMEM/F12 supplemented with 10% fetal bovine serum (FBS; ScienCell Research Laboratory, Carlsbad, CA, USA), 1% penicillin–streptomycin (P/S; Gibco, Carlsbad, CA, USA), and 1% nonessential amino acids (NEAA; Sigma–Aldrich, St. Louis, MO, USA, M7145). The medium was replaced every other day, and the cells were passaged routinely when they reached 80% confluence.

Generation of hESC-derived BVOs

For BVOs induction, hESCs were dissociated into single cells using Gentle Cell Dissociation Reagent (Stem Cell Technologies, 100–0485) for 7 min. On day 0, 2×10^5 cells were pipetted into 15-mL tubes and resuspended in mTeSR medium supplemented with 10 μM Y27632 (Stem Cell Technologies, 72304). Subsequently, the cells were transferred to one well of a poly (2-hydroxyethyl methacrylate) (poly-HEMA; Sigma–Aldrich, St. Louis, MO, USA, P3932, 12 mg/mL)-coated 6-well plate to form embryoid bodies (ESC-EBs). When the ESC-EBs had formed smooth borders on day 1, the mTeSR medium was replaced with N2/B27 medium (50% DMEM/F12 (Gibco), 50% neurobasal medium (Gibco), 2% B27 supplement (Gibco), 1% N2 supplement (Gibco), 0.5% GlutaMAX (Gibco), 0.07% diluted β-mercaptoethanol (1:100, Gibco) and 1% P/S) containing 6 μM CHIR99021 (APE-BIO, USA, A3011) and 30 ng/mL BMP4 (PeproTech, 120-05). The day 4 ESC-EBs were called mesoderm induction-BVOs (MI-BVOs). The MI-BVOs were switched to N2/B27 medium containing 100 ng/mL VEGF-A (Proteintech, HZ-1038) and 2 μM forskolin (Sigma–Aldrich, F3917). The day 7 MI-BVOs were called vascular lineage induction-BVOs (VI-BVOs). The VI-BVOs were embedded in Collagen I (Gibco): Matrigel (3:1) hydrogels and were then incubated for 2 h at 37°C, after which StemPro-34 SFM (Gibco) medium supplemented with 100 ng/mL VEGF-A, 100 ng/mL FGF-2 (PeproTech, 100-18B-100) and 15% FBS was added. The medium was changed after 3 days and every other day thereafter. On day 12, VI-BVOs with abundant vascular networks, called BVOs, could either be directly analyzed or extracted with two sterile 30-gauge needles for maturation into mature BVOs.

Establishment of a high-glucose model for BVOs

To investigate the impact of high glucose on the differentiation levels of MI-BVOs, VI-BVOs and BVOs, we subjected them to a high glucose treatment, with the experimental groups detailed below. MI-BVOs: MI-Control group (17mM glucose (Sigma) + 75mM D-mannitol (Sigma)) and MI-HG group (75mM glucose); VI-BVOs: VI-Control group (17mM glucose +75mM D-mannitol) and VI-HG group (75mM glucose); BVOs: BVOs-Control group (17mM glucose +75mM D-mannitol) and BVOs-HG group (75mM glucose).

Coculture of hucMSC-derived EBs and ESC-derived VI-BVOs

To prepare the cocultures of hucMSC-derived EBs (hucMSC-EBs) and ESC-derived VI-BVOs, hucMSC-EBs and MI-BVOs were collected separately and mixed at a ratio of 1:1 for three consecutive days until the formation of VI-BVOs. The specific steps are as follows: hucMSCs were first dissociated into single cells to generate hucMSC-EBs using trypsin solution for 1 min, after which 1×10^6 cells were pipetted into 15-mL tubes and resuspended in DMEM/F12 supplemented with 10% FBS, 1% P/S, and 1% NEAA. Subsequently, the cells were transferred to one well of a poly-HEMA-coated 6-well plate. When the hucMSC-EBs formed smooth borders, they were cocultured with MI-BVOs in N2/B27 medium supplemented with 100 ng/mL VEGF-A and 2 μM forskolin in poly-HEMA-coated 6-well plates for 3 days.

To eliminate the influence of hucMSCs on VI-BVOs assays, we first select the free VI-BVOs under an inverted phase contrast microscopy with two sterile 30-gauge needles and exclude both free hucMSCs and bound VI-BVOs-hucMSCs.

METHOD DETAILS

Whole-mount immunofluorescence staining

For whole-mount immunofluorescence staining, hucMSC-EBs, ESC-EBs, MI-BVOs, VI-BVOs and BVOs were first collected and then fixed with 4% paraformaldehyde solution overnight at 4°C. After being rinsed with PBS, the above structures were treated with PBS solution containing 3% FBS, 1% bovine serum albumin (BSA; Solarbio) and 0.5% Triton X-100 (Solarbio) for 2 h at room temperature for permeabilization and blocking. After they were thoroughly rinsed with PBS, they were incubated with the following primary antibodies for 12 h at 4°C: rabbit anti-PDGFRβ (1:200, Cell Signaling, Danvers, Massachusetts, USA, 3169S), rabbit anti-COL 4A2 (1:200, Proteintech, 55131-1-AP) Alexa Fluor647 mouse anti-human CD31 (1:100, BD Biosciences, USA, 558094), rabbit anti-Oct-4 Antibody (1:200, Cell Signaling, 2750), mouse anti-SSEA-4 antibody (1:200, Santa Cruz Biotechnology, sc-59368), rabbit anti-PDGFR alpha antibody (1:200, Abcam, ab203491), rabbit anti-VEGF Receptor 2 (FLK1, 1:200, HUABIO, Hangzhou, China, ET1608-33). Negative controls were processed following the same procedures except for incubation with PBS instead of primary antibodies. Alexa Fluor 488-, Alexa Fluor 568- or tetramethylrhodamine isothiocyanate (TRITC)-conjugated goat anti-rabbit/mouse IgG (1:200, Invitrogen, USA) was used as the secondary antibody for a second 12-h incubation at 4°C. Next, the samples were rinsed with PBS three times (20 min/rinse). 4′,6-Diamidino-2-phenylindole (DAPI) (Research Organics, Cleveland, OH) was used to counterstain cell nuclei. Images were acquired via confocal laser scanning microscopy (CLSM; Leica SP8, Heidelberg, Germany).

Acetylated low-density lipoprotein (AcLDL) uptake assay

To evaluate the functional activity of endothelial cells, VI-BVOs and BVOs were harvested and transferred to 1.5-mL tubes. After being rinsed once with DMEM/F12, the VI-BVOs and BVOs were incubated with 10 μg/mL Ac-LDL solution (Invitrogen) at 37°C for 4 h. After the BVOs were rinsed once with DMEM/F12, they were incubated with Hoechst staining solution (1:1000, Beyotime, Shanghai) at 37°C for 30 min.

Hematoxylin-eosin (HE) staining

For evaluation of BVOs by microscopy, BVOs were extracted from the hydrogels with two sterile 30-gauge needles and fixed with 4% paraformaldehyde solution overnight at 4°C. The samples were placed in an embedding box, dehydrated through a graded ethanol series (50%, 70%, 80%, 90%, 100%) and cleared with xylene. Then, the samples were embedded in paraffin and sectioned (to a thickness of 4–6 μm). After deparaffinization with xylene and a graded ethanol series (100%, 90%, 80%, 70%, 50%), the sections were stained with an appropriate concentration of HE solution. After dehydration and clearing, the sections were sealed with neutral resin. Subsequently, images were acquired using a Leica TCS microscope (Wetzlar).

Flow cytometry

VI-BVOs were collected and transferred to 1.5-mL tubes. After being rinsed once with DMEM/F12, the VI-BVOs were dissociated into single cells using collagenase B (Gibco, 1 mg/mL) for 15 min. After the cells were rinsed with DMEM/F12 containing 10% FBS, 2×10^4 cells were pipetted into 1.5-mL tubes and resuspended. The cells were then incubated in a diluted solution containing an Alexa Fluor647-conjugated mouse anti-human CD31 antibody (1:100) and a PE-conjugated mouse anti-human CD140b antibody (BD, Franklin Lakes, NJ, USA, 558821,1:100) for 30 min at 4°C. Fluorescence was detected with a FACSAria flow cytometer (BD), and the fluorescence intensity was analyzed using FlowJo.

Matrigel tube formation assay

To assess the angiogenic potential of endothelial cells derived from VI-BVOs, VI-BVOs were dissociated into single cells and resuspended in StemPro-34 SFM containing 100 ng/mL VEGF-A, 100 ng/mL FGF-2 and 15% FBS. A 96-well plate was prepared and coated with 50 μL of Matrigel/well, and the Matrigel was allowed to polymerize for 30 min at 37°C. A total of 4×10^4 cells/well were pipetted into the precoated 96-well plates. The cells were observed and photographed under an inverted light microscope after 12 h.

Wound-Healing Assay

To assess the horizontal migration capability of vascular cells derived from VI-BVOs, we first dissociated VI-BVOs into single cells and resuspended the cells in StemPro-34 SFM supplemented with 100 ng/mL VEGF-A, 100 ng/mL FGF-2 and 15% FBS. The cells (4×10^4 cells/well) were seeded into a 24-well plate, and the medium was replaced every other day. Approximately five days later, when the cells reach 100% confluence, a sterile 200ul pipette tip was used to scrape the cell monolayer, forming a rectangular cell-free zone in each well. After washing twice with DMEM/F12, the cells were cultured for an additional 24 h following was observed and photographed using an inverted microscope (Carl Zeiss, Gottingen, Germany).

Terminal deoxynucleotidyl transferase dUTP nick end labeling (TUNEL) assay

Apoptosis in vascular cells derived from VI-BVOs was assessed using the One-step TUNEL Apoptosis Assay Kit (Abbkine). We first dissociated VI-BVOs into single cells and resuspended the cells in StemPro-34 SFM medium supplemented with 100 ng/mL VEGF-A, 100 ng/mL FGF-2 and 15% FBS. The cells (4×10^4 cells/well) were seeded into a 24-well plate, and the medium was replaced every other day. After 5 days, the cells were collected and fixed with 4% paraformaldehyde solution overnight at 4°C. After being rinsed with PBS, the cells were treated with PBS containing 3% FBS, 1% BSA and 0.5% Triton X-100 for 2 h at room temperature for permeabilization and blocking. After they were thoroughly rinsed with PBS, they were then incubated with TdT labeling reaction buffer at 37°C in the dark for 2 h. Following the addition of DAPI, the cells were observed and imaged under a fluorescence microscope (Olympus).

3-(4,5-Dimethylthiazol-2-yl)-2,5-diphenyl tetrazolium bromide (MTT) assay

To assess the proliferation of vascular cells derived from VI-BVOs, we first dissociated VI-BVOs into single cells and resuspended the cells in StemPro-34 SFM supplemented with 100 ng/mL VEGF-A, 100 ng/mL FGF-2 and 15% FBS. The cells (5×10^3 cells/well) were seeded into a 96-well plate, and proliferation was assessed by the addition of MTT solution (Invitrogen, 5 mg/mL) on the following day. First, 10 μL of MTT solution was added to each well, and the plate was incubated at 37°C for 4 h, after which the supernatant was discarded. Subsequently, 100 μL of DMSO solution (Thermo Scientific) was added to each well, and the plate was shaken horizontally for 10 min. The contents were then transferred to a new 96-well plate, and the absorbance was measured at 490 nm with a microplate reader (BioTek).

Quantitative PCR (qPCR)

For RNA isolation, ESC-EBs, MI-BVOs, VI-BVOs and BVOs were harvested and transferred to 1.5-mL tubes. After being rinsed with PBS, the BVOs were then immersed in TRIzol solution (Ambion Life Technologies, Denmark) for total RNA extraction. RNA was isolated using the chloroform-isoamyl alcohol method (Domestic analytical purity, Kemio, China), and cDNA was synthesized using a reverse transcription kit (TaKaRa Bio, Dalian, Japan) with oligo dTTTTT primers. SYBR Premix Ex Taq II Kit (Takara Bio)-based qPCR was performed on a CFX384 TouchTM Real-Time PCR Detection System (Bio-Rad) with 35 cycles of amplification. All kits were used following the manufacturers' instructions. The primers were designed using Primer Bank and verified via a Basic Local

Alignment Search Tool (BLAST) search against the *Homo sapiens* genome (ensemble. org). The Cq value of each target gene was normalized to that of the housekeeping gene GAPDH. Primer sequences were as follows.

Western blot analysis

For protein extraction, VI-BVOs were harvested and transferred to 1.5-mL tubes. Total protein was extracted from the VI-BVOs via lysis in radio immunoprecipitation assay (RIPA) buffer (ATWA18021, Abcam) on ice for 5 min, followed by centrifugation at 12,000 rpm for 10 min at 4°C. The protein samples were directly loaded onto a sodium dodecyl sulfate–polyacrylamide gel, separated by electrophoresis and transferred to polyvinylidene difluoride membranes (PVDF, Millipore, Shanghai, China). The membranes were blocked with 5% skim milk in TBST for 2 h at room temperature and were then incubated with primary antibodies overnight at 4°C. Primary antibodies specific for the following proteins were used: *p*-ERK (1:1000, Cell Signaling, 4370), ERK (1:1000, Cell Signaling, 4695), *p*-JNK (1:1000, Cell Signaling, 4668), JNK (1:1000, Cell Signaling, 9252), p-p38 (1:1000, Cell Signaling, 4511), p38 (1:1000, Cell Signaling, 8690), and β-actin (1:1000, Cell Signaling, 4970). After being rinsed with TBST, the membranes were incubated with appropriate horseradish peroxidase (HRP)-conjugated secondary antibodies—anti-rabbit (1:6000; 554021, BD Pharmingen, San Jose, CA, USA) or anti-mouse (1:8000; 554002, BD Pharmingen)—for 1 h at room temperature. The immunoblots were visualized using an Odyssey Infrared Imaging System (LI-COR, USA).

QUANTIFICATION AND STATISTICAL ANALYSIS

Statistical analysis was done using respective tests on GraphPad Prism (version 9.3.1). All reported values were averaged ($n = 3$ replicates per condition from 3 independent experiments) and were expressed as the means ± standard deviations (SD), which is indicated in figure legends. In Figures 1C, 1G, 2F, 3C, 3E, S1, and S2, two-tailed Student's t test was performed to examined grouped differences; In Figure 4E, 5D, 6B, 7B, 7D, S3, and S5, one-way ANOVA was performed to compare quantitative data. Differences were considered statistically significant if $p < 0.05$. * represents $p < 0.05$, ** represents $p < 0.05$, *** represents $p < 0.001$, **** represents $p < 0.0001$.